

Subj.: Re-submission of manuscript nhess-2017-111

Dear Paolo Tarolli,

This cover letter is to go with our electronic re-submission of the manuscript *Criteria for the optimal selection of remote sensing images to map event landslides* by Federica Fiorucci, Daniele Giordan, Michele Santangelo, Furio Dutto, Mauro Rossi, Fausto Guzzetti.

We are grateful to you and to the reviewer for their constructive comments that helped us to improve the work.

In preparing the new version of our work, we considered all the comments and suggestions made by the referee, which were pertinent and helpful.

To respond to the requests of both the reviewers we modified the Abstract, and all the other sections according to the reviewer requests.

We provide a list of our responses to the referee's comments, including details on the changes made to the text.

Overall, we consider this new version of the manuscript significantly improved. We hope the paper can be accepted for publication in the Special Issue: *The use of remotely piloted aircraft systems (RPAS) in monitoring applications and management of natural hazards*.

We look forward to hearing a decision from you soon.

Sincerely,
Federica Fiorucci, on behalf

Answers to Reviewer 3

The paper is an interesting contribution to the journal. However, it should be pointed out more carefully that it is a showcase of a technical application.

AC- We thank the reviewer for pointing out the value of the contribution to the journal. However, we disagree in considering it as a showcase of a technical application, since the experiment was designed to evaluate the impact of images characteristics on landslide mapping. For how the experiment was conceived and developed, the findings are general and applicable to all the cases similar to the setting of the experiment.

Overall, I only have few major points to highlight and some minor issues as they arose during the reading of the research.

1. The title speaks about criteria for the selection of images. However, the criteria are not well defined in the manuscript, and they are only slightly mentioned at the very end of the conclusions. If the point of the manuscript is indeed to present some criteria for selection, these criteria should appear more clearly (e.g. in a list? A well define paragraph?)

AC- In the paper, the criteria are well explained in **Table 3**, and commented in the Discussion section and resumed in the “Concluding remarks” section. The reason why they appear in the “Discussion” section, is that the criteria are a consequence of the results of the experiment. The text in the Discussion section extensively comments on the advantages and limitation of using the different types of images taken into account in the experiment for landslide mapping purposes. The section reads:

“For event landslide mapping, selection between ultra-resolution pseudo-stereoscopic UAV images and very-high resolution stereoscopic satellite images depends on (i) the extent of the investigated area, (ii) the available resources, including time and budget, and (iii) the accessibility to the study area. The selection is largely independent from the landslide signature, at least for landslides similar to the Assignano landslide. From an operational perspective, modern multi-rotor UAVs allow for the acquisition of ultra-resolution images over small areas in a limited time, and at very low costs. UAV-based surveys are flexible in their acquisition planning, and partly independent from the local lighting conditions, including the cloud cover. As a drawback, UAVs are strongly (and negatively) affected by wind speed and weather conditions, they allow for a limited flight time (currently approximately 20 minutes in optimal conditions), which is reduced in bad weather conditions and in cold environments, and typically have limited data storage capacity. Further, it must be possible for the pilot to be at the same time near to the area to be surveyed and to maintain a safe distance from the UAV, a condition that may be difficult to attain in remote or in mountain areas. Collectively, the intrinsic advantages and limitations of modern UAVs make the technology potentially well suited for the acquisition of ultra-resolution images for event, seasonal, and multi-temporal mapping of single landslides, of multiple landslides in a single slope, or in a relatively small area (a few hectares). The use of UAV images was recently proposed by Turner et al. (2015) for determining the landslide dynamics, exploiting time series of images that can be constructed using UAVs. The result is achievable thanks to centimetre co-registration accuracy of the UAV images. Use of UAVs becomes impracticable with the increasing extent of the study area, largely due to (i) the operational difficulty of flying UAVs over large areas (more than a few square kilometres), and (ii) the acquisition and image processing time and associated cost, which increase rapidly with the size of the study area (Table 3). On the other hand, very-high resolution, stereoscopic satellite images have also advantages and limitations for the production of event, seasonal and multi-temporal landslide inventory maps (Guzzetti et al., 2012). The main advantage of the satellite images is that they cover large or very large areas (tens to hundreds of square kilometres) in a single frame with a sub-metre resolution well suited for landslide mapping through the expert visual

interpretation of the images (Ardizzone et al., 2013). On the other hand, limitations remain due to distortions caused by different off-nadir angles in successive scenes, and to difficulties – in places severe – to obtaining suitable (e.g., cloud-free) images at the required time intervals. This is particularly problematic for the production of seasonal and multi-temporal landslide maps. Information on the photographic or morphological signature of the typical, or most abundant, landslides in an area, is important to selecting the optimal characteristics of the images best suited for the production of an event, seasonal or multi-temporal landslide inventory map. Use of images of non-optimal characteristics for a typical landslide signature in an area may condition the quality (completeness, positional and thematic accuracy) of the landslide inventory. Where possible, we recommend that the acquisition of images used for the production of event, seasonal or multi-temporal landslide inventory maps is planned considering the typical landslide signature, in addition to the purpose (event inventory, planning of monitoring systems), scale of the mapping (regional or slope scale), and the size and complexity of the study area (Table 3).”

Moreover, for more clarity we added a text at the end of the “Introduction” section that reads:

“Arguably, the combination of images characteristics, the prevalent landslide signature, the size of the study area, and the available resources define the criteria for the optimal selection of remote sensing images for landslide mapping.”

2. English needs polishing and revision. Many times the authors overuse ‘i.e.’ or they use sentences in a ‘personal’ approach (“we did this”, “we highlight that”, rather than describing what the research indicates), and many sentences are very long and hard to follow.

AC- We thank this Reviewer (R3) for this comment. Most of the ‘i.e.’ were removed, and most of the sentences with a personal approach were converted in an impersonal form. We also revised the text, removing and simplifying the very long sentences.

3. The work does not compare eight maps. It compares seven maps. The dGPS survey is the benchmark (or ground truth), so it is misleading to include it in the list.

AC-Thank you for the suggestion.

The text was modified accordingly.

4. One of the main findings of this work is that a photographic landslide signature is best mapped with higher resolution images, while morphometric signatures are better identified with stereoscopic images. However, the reader does not know what photographic signatures VS morphometric ones are (this is never described in the manuscript).

AC- We thank the Reviewer for this comment. We described more clearly what morphological and photographic signature are in the following sentences (which give also credits of other works in the literature):

In the “Introduction” section we state:

“Heuristic visual mapping of landslide features is based on the systematic analysis of photographic characteristics such as colour, tone, mottling, texture, shape, and morphological characteristics such as size, curvature, concavity and convexity (Pike, 1988). The mentioned photographic and morphological characteristics encompass all the possible landslide features that can be used for the (visual) image interpretation..”

In the “Study area” section, we state:

“The landslide signature (Pike, 1988) is different in the different parts of the landslide. In the source and transportation area the signature is predominantly photographic (radiometric), whereas in the landslide deposit it is mainly morphological (topographic). The photographic signature consists in all the landslide features that can be detected by the analysis of the

photographical characteristics of a given image: colour, tone, pattern and mottling of a given image (Guzzetti et al., 2012). The morphological signature consists in all the landslide features that can be detected by the analysis of the topography, therefore, features such as curvatures, shape, slope, concavity and convexity are always taken into account (Guzzetti et al., 2012). The differences within the landslide allowed to separate the source and transportation area from the deposition area.”

5. *The discussion chapter can be shortened and reorganised; much of it is a repetition of the previous chapter, while the reader would expect to find here some additional considerations about the meaning of the results.*

AC- As suggested by the reviewer, we shortened the discussion section, removing most of the first paragraph. Moreover, to increase the readability of the paragraph, all the values between brackets related to the Error value (a repetition of the results) were removed. Admittedly, we disagree for what concerns the considerations on the meaning of the results, which are quite extensively described in the text.

Minor comments

Abstract

The abstract needs rewording. It should be more research-oriented, and less of a description of the team effort. E.g. first sentence ‘we executed....’ Could be rephrased to ‘this paper presents...’

The work, furthermore, does not compare eight maps, but rather seven different maps as compared to a reference dGPS survey. The so called ‘8th map’, being the ground-truth, is not part of the considered dataset, but it is the benchmark used to compare all the others.

AC-Thanks to R3 for the suggestion. We reorganized the abstract removing most of the personal form sentences.

Lines 19 to 24 report a very long sentence, that needs rephrasing. E.g. “Six maps were obtained through expert knowledge by visual interpretation of images from different sources taken on April 14, 2014. The dataset comprised monoscopic and pseudo-stereoscopic (2.5D) ultra-resolution (0.3 × 0.3 m) images derived using a Canon EOS M photographic camera mounted on a CarbonCore 950 hexacopter, and monoscopic and stereoscopic true-colour and false-colour- composite images (1.84 × 1.84 m resolution) taken by the WorldView-2 satellite.”

AC- In the present version of the abstract this sentence has been removed.

Introduction

Line 48 > ‘to support’ should be changed to ‘supporting the installation of...’

AC-We thank R3 for this suggestion. We corrected the text accordingly.

Line 52 to 58 > “...through field surveys (Santangelo et al., 2010) or the heuristic visual interpretation of monoscopic or stereoscopic aerial or satellite images (Brardinoni et al., 2003; Fiorucci et al., 2011; Ardizzone et al., 2013), of LiDAR-derived images (Ardizzone et al., 2007; Van Den Eeckhaut et al., 2007; Haneberg et al., 2009; Giordan et al., 2013; Razak et al., 2013; Niculita et al., 2016, Petschko et al., 2016), or of ultra-resolution images acquired by Unmanned Aerial Vehicles (UAV, Niethammer et al., 2010, Giordan et al., 2015a, 2015b; Torrero et al., 2015, Turner et al., 2015).

AC-Sincerely, we don’t understand the comment. It seems there is no request/observation.

Line 59 > of the mentioned parameters, which are photographic characteristics, and which ones are morphological? Please explain, also considering that one of the main findings of this work is that a photographic landslide signature is best mapped with higher resolution images, while morphometric signatures are better identified with stereoscopic images.

AC-Correct. We split the sentence in two sentences to clarify what photographic and morphological signatures are. The sentence now reads:

“The heuristic visual mapping of landslide features is based on the systematic analysis of image photographic characteristics such as colour, tone, mottling, texture, shape, and morphological characteristics such as size and curvature, concavity and convexity (Pike, 1988). These photographic and morphological characteristics encompass all the possible landslide features that can be used for the (visual) interpretation of the available imagery.”

Line 66 > maps prepared to exploit one or more of the mentioned techniques are inevitably incomplete. Is that true? Shouldn't we affirm that they “can be” incomplete, rather than making such a strong statement?

AC- We are aware that this statement is strong. But we underline that this is a logical consequence of the consideration that any technique or images have intrinsic limitation. If this is true, this means that these images will be somewhat “blind” for some landslides (e.g., due to the size, type, surrounding land cover), for example due to the spatial or spectral resolution, or lack of three-dimensional information. Nevertheless, we understand that such a strong clause could be better explained and supported in the text. Now, the text quoted by the Reviewer reads:

“All these mapping techniques have inherent advantages and intrinsic limitations, which depend on the characteristics of the images, including their spatial and spectral resolutions (Fiorucci et al., 2011). The limitations affect differently the mapping, based on the size and type of the investigated landslides. As a result, images from single sources or the single mapping techniques are “blind” to some landslides, which inevitably results in incomplete landslide inventory maps. Furthermore, maps also can contain errors in terms of the position, size and shape of the mapped landslides (Guzzetti et al., 2000; Galli et al., 2008, Santangelo et al., 2015a).”

Line 76 > ‘images of different types’ > ‘images from different sources’

AC- We thank R3 for this suggestion. We acknowledge the problem, and we changed the text.

Line 77 > as I mentioned in the abstract, technically you do not compare eight maps, but rather seven maps. The dGPS is the ground truth.

AC-We thank R3 for this suggestion. We corrected accordingly.

Line 80 > on board OF a UAV.

AC- We thank R3 for this suggestion. We corrected the error accordingly.

Study area

Line 96 > “ and A third located...”

AC- We thank R3 for this suggestion. We corrected the error accordingly.

Image acquisition

What software has been used for the SFM technique?

AC- the software used is Agisoft Photoscan. We added this specification in the text.

Line 124: “i.e. the same day...” does not make sense. The same day is not an example, thus, i.e. is not needed

AC- We thank R3 for this suggestion. We removed i.e. from the sentence.

Landslide mapping

Again, you do not compare eight maps. You compare seven maps and use one survey as a benchmark.

Line 147: i.e. is overused. 'who carried out the field activities (the reconnaissance field mapping and the RTK-DGPS survey) were not involved...'

AC- We thank R3 for this suggestion. We removed i.e. from the sentence.

Field mapping

Line 173 again overuse of 'i.e.' > the figure is not an example

AC- We thank R3 for this suggestion. We removed i.e. from the sentence.

Mapping through images

Line 201 again overuse of i.e. > the TC and FCC images are not an example of the images used. They are indeed the images used.

AC- We thank R3 for this suggestion. We removed i.e. from the sentence.

Why the need of draping the UAV image to google earth? The survey itself allows for the creation of a DSM, why using further sources (google) to interpret the images?

AC- The reason why the ultra-high resolution UAV image was draped on Google earth is technological and is explained in the following sentence of section 4.2.:

“To interpret visually the ultra-resolution UAV image, the interpreter overlaid (“draped”) the image on Google Earth™. For the purpose, we first treated the UAV image with the gdal2tiles.py software to obtain a set of image tiles compatible with Google Earth™ terrain visualization platform. To the best of our knowledge, the platform is the only free 2.5D image visualisation environment that allows the editing of vector (point, line, polygon) information. Other commercial (e.g., ArcScene) and open source (e.g., ParaView, GRASS GIS), 2.5D visualization tools do not provide editing capabilities. Google Earth™ is a user-friendly solution for mapping single landslides, and for preparing landslide event inventories for limited areas, with the possibility for the user to visualize a landscape from virtually any viewpoint, facilitating landslide mapping. We refer to the representation of the Assignano landslide obtained through the visual interpretation of the ultra-resolution UAV image as “Map H”.

Results.

Lines 235-238: I disagree. Visually, Fig. 5F is not that different from 5G or H: F underestimates the lower part of the landslide and misses some features in the top part. I would say that visually the most similar is 5E.

AC- We agree that the most similar is the map E as evident also from the value of the error index (fig-). The text was changed accordingly.

Discussion

Lines 318 to 332 are not needed: they are a summary of what has already been said before. I think the whole chapter until line 397 can be shortened because much of it is a repetition of the previous one.

AC- We thank R3 for this suggestion. The suggestion was accepted and the text modified accordingly.

The authors should focus more on either explaining the numbers or discussing them in general as compared to other works or examples.

AC- We thank R3 for this suggestion. However, as stated in the introduction, the literature is rather poor in providing examples of similar studies to be compared to the present work. We cited all the papers in our knowledge:

“Our results are similar to the results of tests performed to compare field-based landslide maps against GPS-based surveys of single landslides (Santangelo et al., 2010), the visual interpretation of very-high resolution stereoscopic satellite images (Ardizzone et al., 2013), or the semi-automatic processing of monoscopic satellite images (Mondini et al., 2013), and confirm the inherent difficulty in preparing accurate landslide maps in the field, unless the mapping is supported by a GPS survey or a similar technology.”

Concluding remarks

Lines 457-468 are not needed. All of this has already been explained throughout the manuscript.

AC- We thank R3 for this suggestion. We removed most of the text as suggested by the reviewer.

Line 465-47 should also be mentioned in the study area description, explaining what photographic and morphological signatures are.

AC-We corrected the text according to the suggestion.

There is no need to explain the results as a list (First....second...third), unless the authors make a short bullet point list of the main findings, and then further discuss them.

AC-We agree, we removed the list.

Line 512 and following. This whole part can be rephrased without using the personal point of view (e.g. We maintain, We emphasise...’ You can simply state that ‘ although the study was conducted on a single landslide, the findings are general and...

AC-We corrected the text according to the suggestion.

[...]. The technique and imagery used to prepare landslide inventory maps should be selected depending on...”

AC- We corrected the text according to the suggestion.

1

2 **Criteria for the optimal selection of remote sensing optical images**

3 **to map event landslides**

4

5 Fiorucci F.¹, Giordan D.², Santangelo M.¹, Dutto F.³, Rossi M.¹, Guzzetti F.¹

6 1 Istituto di Ricerca per la Protezione Idrogeologica, Consiglio Nazionale delle Ricerche, via
7 della Madonna Alta 126, 06128 Perugia, Italy

8 2 Istituto di Ricerca per la Protezione Idrogeologica, Consiglio Nazionale delle Ricerche, Strada
9 delle Cacce 73, 10135 Torino, Italy

10 3 Servizio Protezione Civile della Città Metropolitana di Torino, Via Alberto Sordi 13, 10095
11 Grugliasco, Italy

12

13 Correspondence to: Federica Fiorucci (Federica.Fiorucci@irpi.cnr.it)

14

15

Abstract

Landslides leave discernible signs on the land surface, most of which can be captured in remote sensing images. Trained geomorphologists analyse remote sensing images and map landslides through heuristic interpretation of photographic and morphological characteristics. Despite a wide use of remote sensing images for landslide mapping, no attempt to evaluate how the images characteristics influence landslide identification and mapping exists. This paper presents an experiment to determine the effects of optical image characteristics, such as spatial resolution, spectral content and image type (monoscopic or stereoscopic), on landslide mapping. We considered eight maps of the same landslide in Central Italy: (i) six maps obtained through expert heuristic visual interpretation of remote sensing images, (ii) one map through a reconnaissance field survey, and (iii) one map obtained through a Real Time Kinematic (RTK) differential Global Positioning System (dGPS) survey, which served as a benchmark. The eight maps were compared pairwise and to a benchmark. The mismatch between each maps pair was quantified by the error index, E . Results show that the map closest to the benchmark delineation of the landslide was obtained using the higher resolution image, where the landslide signature was primarily photographic (in the landslide source and transport area). Conversely, where the landslide signature was mainly morphological (in the landslide deposit) the best mapping result was obtained using the stereoscopic images. Albeit conducted on a single landslide, the experiment results are general, and provide useful information to decide on the optimal imagery for the production of event, seasonal and multi-temporal landslide inventory maps.

~~We executed an experiment to determine the effects of optical image characteristics on event landslide mapping. In the experiment, we compared eight maps of the same landslide, the Assignano landslide, in Umbria, Central Italy. Six maps were obtained through the expert visual interpretation of monoscopic and pseudo-stereoscopic (2.5D), ultra-resolution (3×3 cm) images taken on 14 April 2014 by a Canon EOS M photographic camera flown by an CarbonCore 950 hexacopter over the landslide, and of monoscopic and stereoscopic, true colour and false colour composite, 1.84×1.84 m resolution images taken by the WorldView 2 satellite also on 14 April 2014. The seventh map was prepared through a reconnaissance field survey aided by a pre-event satellite image taken on 8 July 2013, available on Google Earth™, and by colour photographs taken in the field with a hand-held camera. The images were interpreted visually by an expert geomorphologist using the StereoMirror™ hardware technology combined with the ERDAS IMAGINE® and Leica Photogrammetry Suite~~

47 ~~(LPS) software. The eighth map, which we considered our reference showing the “ground truth”,~~
48 ~~was obtained through a Real Time Kinematic Differential Global Positioning System (GPS) survey~~
49 ~~conducted by walking a GPS receiver along the landslide perimeter to capture geographic~~
50 ~~coordinates every about 5 m, with centimetre accuracy. The eight maps of the Assignano landslide~~
51 ~~were stored in a Geographic Information System (GIS), and compared adopting a pairwise~~
52 ~~approach. Results of the comparisons, quantified by the error index E , revealed that where the~~
53 ~~landslide signature was primarily photographic (in the landslide source and transport area) the~~
54 ~~best mapping results were obtained using the higher resolution images, and where the landslide~~
55 ~~signature was mainly morphometric (in the landslide deposit) the best results were obtained using~~
56 ~~the stereoscopic images. The ultra-resolution image proved very effective to map the landslide,~~
57 ~~with results comparable to those obtained using the stereoscopic satellite image. Conversely, the~~
58 ~~field-based reconnaissance mapping provided the poorest results, measured by large mapping~~
59 ~~errors, and confirmed the difficulty in preparing accurate landslide maps in the field. Albeit~~
60 ~~conducted on a single landslide, we maintain that our results are general, and provide useful~~
61 ~~information to decide on the optimal imagery for the production of event, seasonal and multi-~~
62 ~~temporal landslide inventory maps.~~

63

64 1 Introduction

65 Accurate detection of ~~single-individual~~ landslides has different scopes, including landslide
66 mapping (Di Maio and Vassallo, 2011; Manconi et al., 2014; Plank et al., 2016), landslide hazard
67 analysis and risk assessment (Allasia et al., 2013), ~~to to support the installations~~support the
68 installation of landslide monitoring systems (Tarchi et al., 2003; Teza et al., 2007; Monserrat and
69 Crosetto, 2008; Giordan et al., 2013), and for landslide geotechnical characterization and
70 modelling (Gokceoglu, 2005; Rosi et al., 2013). Mapping of ~~single-individual~~ landslides can be
71 executed using the same techniques and tools commonly used by geomorphologists to prepare
72 landslide inventory maps ~~i.e., Such techniques and tools includes: a) through~~ field surveys
73 (Santangelo et al., 2010) ~~or, b) the~~ heuristic visual interpretation of monoscopic or stereoscopic
74 aerial or satellite images (Brardinoni et al., 2003; Fiorucci et al., 2011; Ardizzone et al., 2013), c)
75 ~~of~~ LiDAR-derived images (Ardizzone et al., 2007; Van Den Eeckhaut et al., 2007; Haneberg et al.,
76 2009; Giordan et al., 2013; Razak et al., 2013; Niculita et al., 2016, Petschko et al., 2016), ~~or of d)~~
77 ultra-resolution images acquired by Unmanned Aerial Vehicles (UAV, Niethammer et al., 2010,
78 Giordan et al., 2015a, 2015b; Torrero et al., 2015, Turner et al., 2015). ~~The h~~Heuristic visual
79 mapping of landslide features is based on the systematic analysis of ~~image~~ photographic ~~and~~
80 ~~morphological~~ characteristics such as colour, tone, mottling, texture, shape, ~~and morphological~~
81 ~~characteristics such as size, curvature curvature, concavity and convexity~~ (Pike, 1988). ~~These~~ The
82 mentioned photographic and morphological characteristics encompasses all the possible landslide
83 features that can be used for the (visual) image interpretation ~~of the available imagery~~.

84 All these mapping techniques have inherent advantages and intrinsic limitations, which depend on
85 the characteristics of the images, including their spatial and spectral resolutions (Fiorucci et al.,
86 2011). The limitations affect differently the mapping, based on the size and type of the investigated
87 landslides, and on the characteristics of the images, including their spatial and spectral resolutions
88 (Fiorucci et al., 2011). As a result, an a-images of from a single sources or a the single mapping
89 techniques are “blind” to some landslides features. This which inevitably results landslide maps
90 prepared exploiting one or more of the mentioned techniques are inevitably in an incomplete
91 landslide inventory maps incomplete. Furthermore, maps also can, and contain errors in terms of
92 the position, size and shape of the mapped landslides (Guzzetti et al., 2000; Galli et al., 2008,
93 Santangelo et al., 2015a).

94 A ~~few attempts have been made~~exist to evaluate the errors associated to different types of landslide
95 inventory maps (Carrara et al., 1992; Ardizzone et al., 2002, 2007; Van Den Eeckhaut et al., 2007;
96 Fiorucci et al., 2011; Santangelo et al., 2010; Mondini et al., 2013). ~~Most of these attempts~~m
97 compare ~~landslide~~-maps prepared using aerial or satellite images ~~to to maps obtained~~maps obtained
98 through reconnaissance field mapping (Ardizzone et al., 2007; Fiorucci et al., 2011) or GPS
99 surveys (Santangelo et al., 2010). Conversely, only a few authors have attempted to evaluate how
100 the influence of different types of imagerythe characteristics of images acquired from different
101 sources influence on landslide detection and mapping (Carrara et al., 1992).-

102 In this work, we evaluate how images of different types and characteristics influence event
103 landslide mapping. We do ~~this so~~ by comparing ~~eight~~the -maps ~~of a prepared for one single,~~
104 rainfall-induced landslide ~~near the village of Assignano, Umbria, central Italy~~in a pairwise
105 approach, including a benchmark map. The sSeven maps ~~of the same landslide~~ were obtained using
106 different techniques and images, including (i) a reconnaissance field survey, (ii) the interpretation
107 of ultra-resolution images taken by an optical camera on-board ~~of an a~~ UAV, and (iii) the visual
108 interpretation of Very High Resolution (VHR), monoscopic and stereoscopic, multispectral images
109 taken by the WordView-2 satellite. These ~~maps were compared~~comparisons included to an eighth
110 map, obtained through dGPS survey, considered ~~as to be~~ the benchmark showing the “ground truth”
111 ~~i.e., the “true” position, shape and extent of the Assignano landslide~~. Based on the results of the
112 ~~map~~ comparison, we infer the ability of different optical images, with different spectral and spatial
113 characteristics and type (monoscopic or stereoscopic), to portray the landslide features that can be
114 exploited for the visual detection and mapping of landslides. Arguably, the combination of images
115 characteristics, the prevalent landslide signature, the size of the study area, and the available
116 resources define the criteria for the optimal selection of remote sensing images for landslide
117 mapping~~We maintain that the results obtained in our test case are general, and should be considered~~
118 ~~for the optimal selection of images for the detection and mapping event landslides.~~

Formattato: Barrato

119 2 The Assignano landslide

120 For our study, we selected the Assignano landslide, a slide-earthflow (Hutchinson, 1970) triggered
121 by intense rainfall in December 2013 in the northwest-facing slope of the Assignano village,
122 Umbria, central Italy (Fig. 1). The landslide ~~develops~~developed in a crop area, where a layered
123 sequence of sand, silt and clay deposits crop out (Santangelo et al., 2015b). The slope failure is

124 about 340 m long, 40 m wide in the transportation area, and 60 m wide in the deposition area, and
125 is characterized by three distinct source areas, two located on the south-western side of the landslide
126 and a third located on the north-eastern side of the landslide. The source and transportation area
127 has an overall length of about 230 m, and a width increasing from 10 to 40 m from the top of the
128 source area to the bottom of the transportation area. Elevation in the landslide ranges from 276 m
129 along the landslide crown, to 206 m at the lowest tip of the deposit. The source and transportation
130 area is bounded locally by sub-vertical, 2 to 4-m high escarpments. In the landslide, terrain slope
131 averages 11°, and is steeper (12°) in the source and transportation area than in the deposition area
132 (9°). The landslide signature (Pike, 1988) is different in the different parts of the landslide. In the
133 source and transportation area the signature is predominantly photographic (radiometric),
134 whereas in the landslide deposit it is mainly morphometric-morphological (topographic). ~~The~~
135 ~~photographic signature consists in all the landslide features that can be detected by the analysis of~~
136 ~~the photographic characteristics of a given image: colour, tone, pattern and mottling of a given~~
137 ~~image (Guzzetti et al., 2012). The morphological signature consists in all the landslide features that~~
138 ~~can be detected by the analysis of the topography, therefore, features such as curvatures, shape,~~
139 ~~slope, concavity and convexity are always taken into account (Guzzetti et al., 2012). The~~
140 ~~differences within the landslide allowed to separate the source and transportation area from the~~
141 ~~deposition area. differences allow to separate the source and transportation area from the deposition~~
142 ~~area.~~

Formattato: Citation, Italiano (Italia)

Formattato: Citation, Inglese (Regno Unito)

143 3 Image acquisition

144 On 14 April 2014, we conducted an aerial survey of the Assignano landslide using a “X” shaped
145 frame octocopter with eight motors mounted on four arms (four sets of CW and CCW props) with
146 a payload capacity of around one kilogram, and a flight autonomy of about 20 minutes. The UAV
147 was equipped with a remotely controlled gimbal hosting a GoPro Hero 3 video camera and a
148 Canon EOS M camera. We controlled the flight of the UAV manually, relaying on the real-time
149 video stream provided by the GoPro. ~~We kept t~~The operational flight altitude of the UAV ~~was~~
150 ~~kept~~ in the range between 70 and 100 m above the ground. This allowed the Canon EOS M camera
151 to capture 97 digital colour images of the landslide area with a ground resolution of about 2-4 cm,
152 with the single images having an overlap of about 70% and a side-lap of about 40%. For the
153 accurate geocoding of the images, ~~we positioned~~ 13 red-and-white, four-quadrants square targets,

154 20 cm × 20 cm in size ~~were positioned,~~ outside and inside the landslide. ~~We obtained~~ ~~†~~The
155 geographical location (latitude, longitude, elevation) of the 13 target centres was obtained using a
156 Real Time Kinematic (RTK) Differential Global Positioning System (~~DGPS~~~~dGPS~~), ~~—~~with a
157 horizontal error of less than 3 cm. ~~We processed~~ ~~†~~The 97 images were processed using commercial,
158 structure-from-motion software (Agisoft Photoscan) to obtain (i) a 3D point cloud, (ii) a Digital
159 Surface Model (DSM), and (iii) a digital, monoscopic, ultra-resolution (ground sampling distance
160 is 3 × 3 cm) ortho-rectified image in the visible spectral range, which we used for the visual
161 mapping of the Assignano landslide (Table 1).

162 To map the landslide, ~~we also used a~~ ~~a~~ stereoscopic pair of WorldView-2 satellite VHR images
163 ~~taken on 14 April 2014 i.e., the same day of the UAV survey, by the WorldView-2 satellite that~~
164 ~~operates at an altitude of 496 km, was used, and collects~~The satellite stereo pair was taken on 14
165 April 2014 (the same day of the UAV survey). It has a spatial resolution of 46-cm in panchromatic,
166 and 1.84-m in eight band, multispectral, ~~with (coastal blue, blue, green, yellow, red, red edge, and~~
167 ~~near infrared 1, near infrared 2) imagery at a~~ 11-bit dynamic range, ~~in the spectral range 0.400–~~
168 ~~1.040 μm~~. For the satellite imagery, the rational polynomial coefficients (RPCs) ~~are~~ ~~were~~ available,
169 allowing for accurate photogrammetric processing of the images. ~~We used~~ ~~†~~The RPCs were used
170 to generate 3D models of the terrain from the stereoscopic image pair. Exploiting the characteristics
171 of the satellite image, ~~we prepared~~ four separate images for landslide mapping were prepared,
172 namely, (i) a monoscopic, “true colour” (TC) image, (ii) a monoscopic false-colour-composite
173 (FCC) image obtained from the composite near infrared, red and green (band 4,3,2), (iii) a TC
174 stereoscopic pair, and (iv) a FCC stereoscopic pair. ~~We prepared~~ ~~A total of four separate~~-maps of
175 the Assignano landslide were prepared through the visual interpretation of the four images
176 (Table 1). Both satellite and UAV images are free from deep shadows (Fig. 2).

177 To compare the images obtained by the UAV and the WorldView-2 satellite, we co-registered the
178 images, and ~~we~~ evaluated the co-registration on seven control points (Fig. 3), obtaining a Distance
179 Root Mean Square error, DRMS = 0.53 m, and a Circular Error Probability, CEP_{50%} = 0.42 m,
180 which ~~we was~~ considered adequate for landslide mapping, and for the maps comparison.

181 4 Landslide mapping

182 We prepared eight maps of the Assignano landslide using different approaches, images and

Formatted: Figure / Table, Tipo di carattere: Non Grassetto, Italiano (Italia)

183 datasets, including two maps prepared through field surveys, four maps prepared through the visual
184 interpretation of monoscopic and stereoscopic satellite images, and two maps prepared through the
185 visual interpretation of the orthorectified images taken by the UAV (Table 1).

186 The field mapping and the image interpretation were carried out by independent geomorphologists.
187 The two geomorphologists who carried out the field activities (~~i.e.~~, the reconnaissance field
188 mapping and the RTK-~~DGPS~~-~~dGPS~~ survey), were not involved in the visual interpretation of the
189 satellite and the UAV images. Equally, the geomorphologist who interpreted visually the satellite
190 and the UAV images did not take part in the field activities. Visual interpretation of the remotely-
191 sensed images was performed by a single geomorphologist to avoid problems related to different
192 interpretation skills by different interpreters (Carrara et al., 1992). ~~We then compared~~ The eight
193 ~~resulting~~ maps of the Assignano landslide were then compared adopting a pairwise approach to
194 quantify and evaluate the mapping differences.

195 The geomorphologist who interpreted visually the images was shown first the 1.84-m resolution,
196 monoscopic satellite image, next the 1.84-m resolution stereoscopic satellite pair, and lastly the 3-
197 cm resolution UAV images. The monoscopic and the stereoscopic satellite images were first shown
198 in TC and then in FCC. Lastly, the interpreter was shown the draped ultra-resolution UAV image.
199 Selection of the sequence of the images given to the geomorphologist for the expert driven visual
200 interpretation was based on the assumption that for landslide mapping (i) the ultra-resolution
201 monoscopic images provide more information than the 1.84-m monoscopic or stereoscopic images,
202 (ii) for equal spatial resolution images, stereoscopic images provide more information than
203 monoscopic images, and (iii) for equal image type (monoscopic, stereoscopic), the FCC images
204 provide more information than the TC images. To prevent biases related to a possible previous
205 knowledge of the landslide, the interpreter was not shown the results of the reconnaissance field
206 mapping.

207 4.1 Field mapping

208 Field mapping of the Assignano landslide consisted in two synergic activities, (i) a reconnaissance
209 field survey, and (ii) a RTK ~~DGPS~~-~~dGPS~~ aided survey. First, the reconnaissance field survey was
210 conducted by two geomorphologists (FF and MR) who observed the landslide and took
211 photographs of the slope failure from multiple viewpoints, close to and far from the landslide. The
212 geomorphologists ~~draw~~-drew in the field a preliminary map of the landslide exploiting the most

213 recent satellite image available at the time in Google Earth™, which was a pre-event image taken
214 on 8 July 2013 ~~i.e. (Fig. 4), before the landslide occurred~~. The reconnaissance field mapping was
215 then refined in the laboratory using the ground photographs taken in the field. We refer to this
216 reconnaissance representation of the Assignano landslide as “Map B”.

217 Next, the same two geomorphologists (FF and MR) conducted an RTK ~~DGPS~~dGPS aided survey
218 walking a Leica Geosystems GPS 1200 receiver along the landslide boundary, capturing 3D
219 geographic coordinates every about 5 m, in 3D distance. For the purpose, ~~we used t~~he SmartNet
220 ItalPoS real-time network service was used to transmit the correction signal from the GPS base
221 station to the GPS roving station. The estimated accuracy obtained for each survey point measured
222 along the landslide boundary was 2 to 5 cm, measured by the root mean square error (RMSE), on
223 the ETRF-2000 reference system. ~~We refer to t~~The cartographic representation of the Assignano
224 landslide produced by the RTK ~~DGPS~~dGPS survey is referred to as “Map A”, and is. ~~We~~
225 ~~considered this map~~ as the “ground truth”, ~~and we use it as a~~ benchmark against which to compare
226 the other maps. ~~We acknowledge that m~~Mapping a landslide by walking a GPS receiver around its
227 boundary is an error prone operation e.g., because in places the landslide boundary is not sharp, or
228 clearly visible from the ground (Santangelo et al., 2010). ~~However~~Nevertheless, we maintain this
229 is the most reasonable working assumption (Santangelo et al., 2010). ~~Furthermore, and that~~ the
230 geometrical information obtained by walking a GPS receiver along the landslide boundary was
231 superior to the information obtained through the reconnaissance field mapping (Map B)
232 (Santangelo et al., 2010).

233 4.2 Mapping through image interpretation

234 A trained geomorphologist (MS) used the three monoscopic images (~~i.e.,~~ the TC and FCC
235 monoscopic satellite images, and the monoscopic ultra-resolution UAV image) to perform a
236 heuristic, visual mapping of the Assignano landslide. For this purpose, the interpreter considered
237 the photographic (colour, tone, mottling, texture) and ~~geometrical-geometric~~ (shape, size,
238 ~~curvature,~~ pattern of individual terrain features, or sets of features) characteristics of the images
239 (Antonini et al., 1999). In this way, the geomorphologist prepared (i) “Map C” interpreting visually
240 the monoscopic, TC satellite image, (ii) “Map D” interpreting visually the monoscopic, FCC
241 satellite image, and (iii) “Map G” interpreting visually the monoscopic, TC UAV image (Table 1).

242 Next, the interpreter used the two stereoscopic satellite images (~~i.e.,~~ the TC and FCC images) to

243 prepare “Map E” and “Map F” (**Table 1**). In the stereoscopic images, the photographic and
244 morphological information is combined, favouring the recognition of the landslide features through
245 the joint analysis of photographic (colour, tone, mottling, texture), geometrical (shape, size, pattern
246 of features), and morphological terrain features (curvature, convexity, concavity). To analyse
247 visually the stereoscopic satellite images, the interpreter used the StereoMirror™ hardware
248 technology, combined with the ERDAS IMAGINE® and Leica Photogrammetry Suite (LPS)
249 software. To map the landslide features in real-world, 3D geographical coordinates, the interpreter
250 used a 3D floating cursor (Fiorucci et al., 2015).

251 ~~To interpret the ultra-resolution UAV image, the interpreter overlaid (“draped”) the image on~~
252 ~~Google Earth™. For the purpose, we first treated the UAV image with gdal2tiles.py software to~~
253 ~~obtain a set of image tiles compatible with the Google Earth™ terrain visualization platform.~~ To
254 interpret visually the ultra-resolution UAV image, the interpreter overlaid (“draped”) the image on
255 Google Earth™. For the purpose, we first treated the UAV image with the gdal2tiles.py software
256 to obtain a set of image tiles compatible with Google Earth™ terrain visualization platform. To the
257 best of our knowledge, the platform is the only free, 2.5D image visualisation environment that
258 allows the editing of vector (~~i.e.~~, point, line, polygon) information. Other commercial (e.g.,
259 ArcScene) and open source (e.g., ParaView, GRASS GIS), 2.5D visualization tools do not provide
260 editing capabilities. Google Earth™ is a user-friendly solution for mapping single landslides, and
261 for preparing landslide event inventories for limited areas, with the possibility for the user to
262 visualize a landscape from virtually any viewpoint, facilitating landslide mapping. ~~We refer to t~~The
263 representation of the ~~Assignano~~ landslide obtained through the visual interpretation of the ultra-
264 resolution UAV image is referred to as “Map H”.

265 For the visual interpretation of the satellite and the UAV images, the interpreter adopted a
266 visualization scale in the range from 1:1000 to 1:6000, depending on the image spatial resolution
267 (**Table 1**). The scale of observation was selected to obtain the best readability of each landslide
268 feature and the surroundings, ~~which is a common practice in image visual analysis for landslide~~
269 ~~mapping (Fiorucci et al., 2011). Hence, e~~Despite ~~ven if~~ the maps were produced at slightly different
270 observation scales, the differences arising from the comparison are due to actual features (e.g.i.e.,
271 the image resolution and radiometry), and not to the different observation scales.

272 5 Results

273 Using the described mapping methods, and the available satellite and UAV images (Table 1), we
274 prepared eight separate and independent cartographic representations of the Assignano landslide,
275 shown in Fig. 5 as Map A to Map H.

276 Considering the entire landslide, visual inspection of Fig. 5 reveals that the maps most similar to
277 the benchmark (Map A) ~~are~~ is Map E, prepared examining the true colour (TC) stereoscopic
278 satellite image, ~~and Map F, prepared examining the false colour composite (FCC) stereoscopic~~
279 ~~satellite image.~~ Conversely, the largest differences were observed for the landslide maps obtained
280 through the reconnaissance field survey (Map B), and the visual interpretation of the monoscopic
281 satellite images (Map C and Map D). Considering only the source and transportation areas (dark
282 colours in Fig. 5), interpretation of the UAV ultra-resolution images resulted in the landslide maps
283 most similar (Map G and Map H) to the benchmark (Map A). It is worth noticing the systematic
284 lack in the mapping of one of the two secondary landslide source areas located in the SW side of
285 the landslide, which was recognized only from the visual inspection of the ultra-resolution
286 orthorectified images taken by the UAV. In the field, this secondary source area was characterized
287 by small cracks along the escarpment and a limited disruption of the meadow, making it particularly
288 difficult to be detected and mapped. We argue that only the ultra-resolution images allowed for the
289 detection of the cracks. Considering only the landslide deposit (light colours in Fig. 5), the
290 landslide mapping that was more similar to the benchmark (Map A) was obtained interpreting the
291 TC, stereoscopic satellite images (Map E). We also note that in most of the maps the landslide
292 deposit was mapped larger (Map G, Map H) or much larger (Map B, Map C and Map D) than the
293 benchmark (Map A).

294 Table 2 lists geometric measures of the mapped landslides, including the planimetric measurement
295 of length, width and area (i) of the entire landslide, (ii) of the landslide source and transportation
296 area (dark colours in Fig. 5), and (iii) of the landslide deposit (light colours in Fig. 5). The length
297 and width measurements were obtained in a GIS as the length and the width of the minimum
298 oriented rectangle encompassing (i) the entire landslide, (ii) the landslide source and transportation
299 area, and (iii) the landslide deposit. Our benchmark (Map A) has a total area $A_L = 1.1 \times 10^4 \text{ m}^2$, and
300 is $L_{LS} = 362 \text{ m}$ long and $W_{LS} = 71 \text{ m}$ wide. Amongst the other seven maps (Map B to Map H in
301 Fig. 5), the largest landslide is shown in Map B, obtained through the reconnaissance field

302 mapping, and has $A_L = 1.91 \times 10^4 \text{ m}^2$, 71.1% larger than the benchmark. Conversely, the smallest
 303 landslide is shown in Map F, with $A_L = 1.1 \times 10^4 \text{ m}^2$, 4.6% smaller than the benchmark. The longest
 304 and largest landslide is found in Map C, with $L_{LS} = 405 \text{ m}$ (11% longer than the benchmark) and
 305 $W_{LS} = 113 \text{ m}$ (60% wider than the benchmark).

306 Considering the source and transportation area, in Map A (the benchmark) $A_{LS} = 5.4 \times 10^3 \text{ m}^2$,
 307 $L_{LS} = 228 \text{ m}$, and $W_{LS} = 52 \text{ m}$. The largest representation of the source and transportation area is
 308 found in Map B (reconnaissance field mapping) with $A_{LS} = 7.4 \times 10^3 \text{ m}^2$, 36.9% larger than the
 309 benchmark, and the smallest source and transportation area is found in Map G, with
 310 $A_{LS} = 5.2 \times 10^3 \text{ m}^2$, 3.6% smaller than the benchmark. The longest source and transportation area is
 311 found in Map F, with $L_{LS} = 239 \text{ m}$, 5% longer than the benchmark, and the shortest source and
 312 transportation area is shown in Map C, with $L_{LS} = 206 \text{ m}$, 9.7% shorter than the benchmark. The
 313 largest source and transportation area is shown in Map B, $W_{LS} = 60 \text{ m}$, 15.7% wider than Map A,
 314 and the narrowest source and transportation area is in Map C, $L_{LS} = 44 \text{ m}$, 15.3% narrower than the
 315 benchmark. Considering instead only the landslide deposit, our benchmark (Map A) has
 316 $A_{LD} = 5.7 \times 10^3 \text{ m}^2$, $L_{LS} = 153 \text{ m}$, and $W_{LS} = 61 \text{ m}$. The largest deposit is shown in Map B
 317 (reconnaissance field mapping) and has $A_{LD} = 1.2 \times 10^4 \text{ m}^2$, 103.4% larger than the benchmark,
 318 whereas the smallest landslide deposit is shown in Map F, with $A_{LD} = 4.6 \times 10^3 \text{ m}^2$, 19.8% smaller
 319 than the benchmark. Analysis of the length and width of the landslide deposit reveals that Map C
 320 shows the longest deposit, $L_{LS} = 206 \text{ m}$, 35% longer than the benchmark, and Map H shows the
 321 shortest deposit, $L_{LS} = 122 \text{ m}$, 20.2% shorter than the benchmark. Similarly, the largest landslide
 322 deposit is shown in Map C, $W_{LS} = 112 \text{ m}$, 82.8% wider than the benchmark, and the narrowest
 323 landslide deposit is portrayed in Map E, $W_{LS} = 56 \text{ m}$, 8.2% less than the benchmark.

324 To compare quantitatively the different landslide maps, we use the error index E proposed by
 325 Carrara et al. (1992), adopting the pairwise comparison approach proposed by Santangelo et al.
 326 (2015a). The index provides an estimate of the discrepancy (or similarity) between corresponding
 327 polygons in two maps, and is defined as:

$$E = \frac{(A \cup B) - (A \cap B)}{(A \cup B)}; 0 \leq E \leq 1, \quad (1)$$

328 where, A and B are the areas of two corresponding polygons in the compared maps, and \cup and \cap
 329 are the geographical (geometric) union and intersection of the two polygons, respectively. E spans

330 the range from 0 (perfect matching) to 1 (complete mismatch).

331 We compared the eight maps of the Assignano landslide (Fig. 5) adopting a pairwise approach,
332 and considering first only the landslide source and transportation area, next only the landslide
333 deposit, and lastly the entire landslide. Fig. 6 summarizes the 84 values of the error index E , 28 for
334 the landslide source and transportation area (Fig. 6 I), 28 for the landslide deposit (Fig. 6 II), and
335 28 for the entire landslide (Fig. 6 III). On average, the source and transportation area exhibits
336 values of the error index smaller than the values found in the landslide deposit. This indicates that
337 in the source and transportation area the landslide maps are more similar than in the landslide
338 deposit. Inspection of Fig. 6 I, reveals a decrease of the error index in the source and transportation
339 area for the maps obtained interpreting the available images (from Map C to Map H), compared to
340 our benchmark obtained through the RTK ~~DGPS~~dGPS survey ($0.15 \leq E \leq 0.38$), with Map G
341 obtained interpreting the TC, monoscopic, ultra-resolution UAV image. In the landslide deposit
342 (Fig. 6 II), the minimum difference ($E = 0.21$) was found comparing the benchmark to Map E,
343 obtained through the interpretation of the stereoscopic TC satellite image, and the largest difference
344 ($E = 0.52$) was found comparing the benchmark to Map C, prepared interpreting the TC,
345 monoscopic, satellite image.

346 Comparison of the maps obtained through the interpretation of the monoscopic images (Map C and
347 Map D), and the maps obtained through the interpretation of stereoscopic (Map E and Map F) or
348 ultra-resolution images (Map G and Map H), reveals high values of the error index, which is
349 slightly worse in the landslide deposit. This is evident in the source and transportation area
350 ($0.31 \leq E \leq 0.44$) (Fig. 6 I), and in the landslide deposit ($0.43 \leq E \leq 0.63$) (Fig. 6 II). Map C and
351 Map D are very similar, with a mapping error $E = 0.17$. Maps obtained through the interpretation
352 of stereoscopic satellite images (Map E and Map F, prepared using TC and FCC images,
353 respectively), and maps prepared by interpreting the UAV images (Map G and Map H), exhibit a
354 generally low value of E . In particular, $0.14 \leq E \leq 0.26$ in the landslide source and transportation
355 area, and $0.15 \leq E \leq 0.38$ in the landslide deposit. The reconnaissance field mapping (Map B)
356 exhibited the largest differences compared to all the other maps ($0.63 \leq E \leq 0.45$) in the landslide
357 source and transportation area, and $0.44 \leq E \leq 0.73$ in the landslide deposit. The large values of E
358 in the landslide deposit is probably due to lack of visibility of part of the landslide toe in the field.

359 6 Discussion

360 ~~In this section, we discuss the~~ ability of the different images ~~used to detect and map the~~
361 ~~Assignano landslide (Fig. 1)~~ to resolve the landslide photographic and morphological signatures
362 ~~is discussed~~, considering separately (i) the image spatial and (ii) spectral resolutions, and the (iii)
363 image type ~~i.e.~~, (monoscopic, stereoscopic, or pseudo-stereoscopic). ~~We treat each of the these~~
364 three factors ~~is considered~~ separately, keeping the other two factors constant. ~~To evaluate the~~
365 ~~influence of the image spatial resolution on landslide mapping, we compare to our benchmark~~
366 ~~(Map A) two true colour (TC) monoscopic maps (Map C and Map G), and two TC stereoscopic~~
367 ~~maps (Map E and Map H). Next, to evaluate the influence of the image spectral resolution on the~~
368 ~~landslide mapping, we compare to the benchmark (Map A) the TC and the false colour composite~~
369 ~~(FCC) monoscopic maps (Map C and Map D), and the corresponding TC and FCC stereoscopic~~
370 ~~maps (Map E and Map F). Lastly, to assess the influence of the type of image (i.e., monoscopic,~~
371 ~~stereoscopic, pseudo-stereoscopic) on the landslide mapping, we compare to the benchmark~~
372 ~~(Map A) the monoscopic (Map C) and the stereoscopic (Map E) TC maps (Fig. 7A), the two FCC~~
373 ~~maps (Map D and Map F) (Fig. 7B), and the maps obtained interpreting the ultra-resolution images~~
374 ~~captured by the UAV (Map G and Map H). Fig. 6 summarizes the mapping errors E obtained by~~
375 ~~the pairwise comparisons of the eight landslide maps shown in Fig. 5.~~

376 ~~We first evaluate the role of the image spatial resolution in the production of the different maps of~~
377 ~~the Assignano landslide.~~ Inspection of Fig. 6 I reveals that the maps of the landslide source and
378 transportation area obtained from images characterized by the highest spatial resolution (~~i.e.~~,
379 Map G and Map H) exhibits the smallest errors (~~$E \leq 0.16$~~), when compared to the benchmark
380 ~~(Map A)~~. The mapping error obtained for Map C (TC, monoscopic, ~~$E = 0.38$~~) is 2.5 times larger
381 than the error obtained using the ultra-resolution orthorectified images taken by the UAV (~~Map G,~~
382 ~~$E = 0.15$, and Map H, $E = 0.16$~~), whereas the error obtained from Map E (TC, stereoscopic,
383 ~~$E = 0.23$~~) is smaller, and about 1.5 times larger than the error obtained for Map H (TC, pseudo-
384 stereoscopic, ~~$E = 0.16$~~). In the landslide deposit (Fig. 6 II), the map obtained exploiting the
385 monoscopic, TC satellite image ~~(Map C)~~ exhibits an error ~~$E = 0.52$~~ , 1.7 times larger than the error
386 obtained using Map G (TC, monoscopic UAV, ~~$E = 0.30$~~). Conversely, the error is smaller in the
387 map obtained from the 2-m spatial resolution, stereoscopic TC satellite image (Map E, ~~$E = 0.21$~~)
388 than from the 3-cm spatial resolution, pseudo-stereoscopic image taken by the UAV (Map H,

389 ~~$E=0.30$~~). Collectively, the pairwise comparisons highlights an improvement of the quality of the
390 mapping of the landslide features that exhibits a distinct photographic signature, most visible in
391 the source and transportation area of the Assignano landslide, with an increase of the image spatial
392 resolution (Fig. 6). Use of the ultra-resolution image captured by the UAV did not result in an
393 improvement of the mapping in the deposition area of the Assignano landslide, where the landslide
394 exhibits a distinct morphological signature. ~~We furthermore, observe that~~ most of the landslide
395 parts that were not identified in the maps prepared using the satellite image are covered by
396 vegetation, locally bounded by small and thin cracks with an average width smaller than the size
397 of the 2×2 m pixel. In the satellite image, the cracks are located in pixels containing a mix of
398 vegetation and bare soil, making it difficult for the interpreter to recognize the cracks.

399 Next, we evaluate the effectiveness of the image spectral resolution, and for the purpose we
400 examine the mapping errors of Maps C and Map E (TC), and of Map D and Map F (FCC). The
401 mapping of the source and transportation area prepared using the false-colour-composite (FCC)
402 images (Map D and Map F) resulted in smaller errors than the mapping prepared using the
403 corresponding true-colour (TC) images (Map C and Map E), for both monoscopic and stereoscopic
404 images (Fig. 6 I). In the source and transportation area, the false-colour-composite emphasized the
405 presence or absence of the vegetation, and contributed locally to highlight the typical
406 photographic signature of the landslide, ~~which helped the photo interpreter to detect and map the~~
407 ~~slope failure~~. Conversely, in the landslide deposition area (Fig. 6 II) use of the FCC images did not
408 result in a systematic reduction of the mapping error, when compared to the TC images. We
409 conclude that use of the additional information contributed by the Near Infrared (NIR) band in the
410 1.84-m resolution satellite image did not improve the quality of the mapping. On the other hand,
411 the contribution of the NIR in the 3-cm UAV image remains unknown.

412 ~~Next~~ ~~Lastly, we evaluate~~ the influence of the image type (~~i.e.~~, monoscopic, stereoscopic, pseudo-
413 stereoscopic) on the mapping error was evaluated by comparing (i) the TC images (Map C and
414 Map E), (ii) the FCC images (Map D and Map F), and (iii) the ultra-resolution UAV image (Map G
415 and Map H). Comparison of the TC, monoscopic (Map C) and stereoscopic (Map E) images
416 revealed a mapping error for the entire landslide ~~$E=0.48$~~ , with the mismatch larger in the
417 deposition area (~~$E=0.59$~~) than in the source and ~~transpiration-transportation~~ area (~~$E=0.45$~~)
418 (Fig. 6). A similar result was obtained comparing the FCC, monoscopic (Map D) and stereoscopic

Formattato: Barrato

419 (Map F) images, with a mapping error for the entire landslide $E=0.44$, and again the mismatch is
420 larger in the deposition area ($E = 0.60$) than in the source and transportation area ($E = 0.36$). In the
421 deposition area, where the morphological signature of the Assignano landslide is strongest, the
422 mapping error obtained comparing ~~our~~ the benchmark (Map A) to the landslide maps prepared
423 using the monoscopic images (Map C and Map D) is 2 times larger than the error observed for the
424 maps prepared using the corresponding stereoscopic images (Map E and Map F). The differences
425 are smaller in the source and transportation area, where the morphological signature of the landslide
426 is less distinct. ~~Direct~~ comparison of Map E (TC, stereoscopic) and Map F (FCC, stereoscopic)
427 for the entire landslide reveals a very small mapping error ($E=0.15$), indicating the similarity of
428 the two maps, which were also very similar to the benchmark (Map A), $E \leq 0.20$.

429 Comparison for the entire landslide of the maps prepared using the ultra-resolution images captured
430 by the UAV (Map G and Map H) exhibits the smallest error of all the pairwise comparisons
431 ($E=0.08$) (Fig. 6 III), indicating the large degree of matching between the two maps. The degree
432 of matching is only marginally smaller in the source and transportation area, and in the deposition
433 area ($E=0.15$). When compared to ~~our~~ the benchmark (Map A), Map G and Map H exhibit a small
434 error ($E=0.19$) for the entire landslide, which is larger in the deposition area ($E \leq 0.30$) and slightly
435 smaller in the source and transportation area ($E \leq 0.15$). Interestingly, the mismatch with Map A
436 (the benchmark) is lower for the monoscopic (Map G) than for the pseudo-stereoscopic (Map H)
437 map. The finding highlights the lack of an advantage in using a pseudo-stereoscopic (2.5D) image
438 for mapping the ~~Assignano~~ landslide. We attribute this result to the low resolution of the (pre-
439 event) DEM used to drape the ultra-resolution image for visualization purposes, which did not add
440 any significant morphological information to the expert visual interpretation.

441 Joint analysis of Fig. 5B and Fig. 6 reveals that, when compared to ~~our~~ the benchmark (Map A),
442 the reconnaissance field mapping (Map B) exhibited the largest mapping error of all the performed
443 pairwise comparisons, with $E = 0.45$ in the source and transportation area, $E = 0.67$ in the landslide
444 deposit, and $E = 0.55$ for the entire landslide. ~~We note that an error of $E=0.50$ indicates that 50%~~
445 ~~of the landslide area in one map (Map B, in this case) does not overlay with the other map (Map A,~~
446 ~~the benchmark, in this case).~~ Our results are similar to the results of tests performed to compare
447 field-based landslide maps against GPS-based surveys of single landslides (Santangelo et al.,
448 2010), the visual interpretation of very-high resolution stereoscopic satellite images (Ardizzone

449 et al., 2013), or the semi-automatic processing of monoscopic satellite images (Mondini et al.,
450 2013), and confirm the inherent difficulty in preparing accurate landslide maps in the field, unless
451 the mapping is supported by a GPS survey or a similar technology.

452 ~~Our~~The experiment showed that the mapping of the Assignano landslide obtained exploiting the
453 ultra-resolution images captured by the UAV (Map G and Map H) was comparable to the maps
454 obtained using the high resolution stereoscopic satellite image (Map E and Map F), and to the
455 ground-based RTK ~~DGPS~~dGPS survey (Map A, the benchmark). ~~The~~ We conclude that ultra-
456 resolution images ~~captured by an UAV~~ and the stereoscopic satellite images are well suited to
457 map event landslides, at least in physiographical settings similar to the one of ~~our~~ this study area,
458 and for landslides similar to the Assignano landslide (~~slide-earthflow~~Fig. 1). -

459 For event landslide mapping, selection between ultra-resolution pseudo-stereoscopic UAV images
460 and very-high resolution stereoscopic satellite images depends on (i) the extent of the investigated
461 area, (ii) the available resources, including time and budget, and (iii) the accessibility to the study
462 area. The selection is largely independent from the landslide signature, at least for landslides similar
463 to the Assignano landslide. From an operational perspective, modern multi-rotor UAVs allow for
464 the acquisition of ultra-resolution images over small areas in a limited time, and at very low costs.
465 UAV-based surveys are flexible in their acquisition planning, and partly independent from the local
466 lighting conditions, including the cloud cover. As a drawback, UAVs are strongly (and negatively)
467 affected by wind speed and weather conditions, they allow for a limited flight time (currently
468 approximately 20 minutes in optimal conditions), which is reduced in bad weather conditions and
469 in cold environments, and typically have limited data storage capacity. Further, it must be possible
470 for the pilot to be at the same time near to the area to be surveyed and to maintain a safe distance
471 from the UAV, a condition that may be difficult to attain in remote or in mountain areas.
472 Collectively, the intrinsic advantages and limitations of modern UAVs make the technology
473 potentially well suited for the acquisition of ultra-resolution images for event, seasonal, and multi-
474 temporal mapping of single landslides, of multiple landslides in a single slope, or in a relatively
475 small area (a few hectares). The use of UAV images was recently proposed by Turner et al. (2015)
476 for determining the landslide dynamics, exploiting time series of images that can be constructed
477 using UAVs. The result is achievable thanks to centimetre co-registration accuracy of the UAV
478 images. Use of UAVs becomes impracticable with the increasing extent of the study area, largely

479 due to (i) the operational difficulty of flying UAVs over large areas (more than a few square
480 kilometres), and (ii) the acquisition and image processing time and associated cost, which increase
481 rapidly with the size of the study area (Table 3). On the other hand, very-high resolution,
482 stereoscopic satellite images have also advantages and limitations for the production of event,
483 seasonal and multi-temporal landslide inventory maps (Guzzetti et al., 2012). The main advantage
484 of the satellite images is that they cover large or very **large** areas (tens to hundreds of square
485 kilometres) in a single frame with a sub-metre resolution well suited for landslide mapping through
486 the expert visual interpretation of the images (Ardizzone et al., 2013). On the other hand,
487 limitations remain due to distortions caused by different off-nadir angles in successive scenes, and
488 to difficulties – in places severe – to obtaining suitable (e.g., cloud-free) images at the required
489 time intervals. This is particularly problematic for the production of seasonal and multi-temporal
490 landslide maps. Information on the photographic or morphological signature of the typical, or most
491 abundant, landslides in an area, is important to selecting the optimal characteristics of the images
492 best suited for the production of an event, seasonal or multi-temporal landslide inventory map. Use
493 of images of non-optimal characteristics for a typical landslide signature in an area may condition
494 the quality (i.e., completeness, positional and thematic accuracy) of the landslide inventory. Where
495 possible, we recommend that the acquisition of images used for the production of event, seasonal
496 or multi-temporal landslide inventory maps is planned considering the typical landslide signature,
497 in addition to the purpose (event inventory, planning of monitoring systems), scale of the mapping
498 (i.e., regional or slope scale), and the size and complexity of the study area (Table 3).

499 7 Concluding remarks

500 ~~We executed an~~The experiment aimed at determining and measuring the effects of the image
501 characteristics on event landslide mapping. ~~In the experiment, we compared landslide maps~~
502 ~~obtained (i) through the expert visual interpretation of an ultra resolution image taken by an UAV~~
503 ~~with a ground resolution of 3×3 cm, and monoscopic and stereoscopic true colour and false~~
504 ~~colour composite (1.84×1.84 m) images taken by the WorldView 2 satellite, (ii) a reconnaissance~~
505 ~~field survey of the landslide, and (iii) an accurate survey of the landslide obtained by walking a~~
506 ~~GPS receiver along the landslide boundary. We conducted the experiment on a~~The study was
507 ~~conducted on a slide-earthflow the Assignano landslide (Fig. 1) triggered by intense rainfall in~~
508 December 2013 in the northwest-facing slope of the Assignano village, Umbria, central Italy. The

509 landslide exhibited a predominant photographic (radiometric) signature in the source and
510 transport area, and a more distinct morphological (topographic) signature in the deposition area.

511 ~~The results of our mapping experiment allow for the following conclusions.~~

512 Increasing the spatial resolution allows to reduce the error of landslide mapping where landslides
513 show mainly a photographic signature. Such a behaviour was observed in the First, in the
514 landslide source and transport area, where the signature of the slope failure was primarily
515 photographic (radiometric), mapping errors (Carrara et al., 1992; Santangelo et al., 2015a)
516 decreased with the increase of the spatial resolution of the images used for the expert visual
517 detection and mapping of the landslide. In the same areaHere, the image photographic (radiometric)
518 characteristics (true-colour, false-colour-composite) and the image type (monoscopic,
519 stereoscopic) played a minor role in augmenting the quality of the landslide maps. Conversely, in
520 the deposition area, where the signature of the landslide was primarily morphological
521 (topographical), mapping errors decreased using stereoscopic satellite images that allowed
522 detecting topographic features distinctive of the landslide.

523 FCC and TC in the stereoscopic satellite images give similar values of the error. This indicates that
524 the spectral resolution of the images does not provide useful information to recognize and map the
525 landslide morphological features. On the other hand, the high spatial resolution provided by the
526 UAV images reduces the error, when compared to the monoscopic satellite imagery. However, the
527 error obtained using the UAV images remains higher than that obtained using stereoscopic satellite
528 images, despite the latter having a pixel one order of magnitude larger than the UAV images. We
529 conclude that the increase in the spatial resolution improves the ability to map morphological
530 features when using monoscopic images.

531 ~~Second, use~~Use of the stereoscopic satellite images resulted in more accurate landslide maps (lower
532 error index E) than the corresponding monoscopic images in the landslide deposition area, where
533 the signature of the landslide was primarily ~~morphometric-morphological~~(topographic). This was
534 expected, as the stereoscopic vision allowed to better capture the 3D terrain features typical of a
535 landslide (Pike, 1988), including curvature, convexity and concavity. Conversely, visual
536 examination of the false-colour-composite images resulted in more accurate maps than the
537 corresponding true-colour images in the landslide source and transport area, where the signature of
538 the landslide was primarily photographic ~~(radiometric)~~. This was also expected (Guzzetti et al.,

539 ~~2012~~). Expert visual interpretation of pseudo-stereoscopic ultra-resolution image failed to provide
540 better results than the corresponding monoscopic ultra-resolution image, most probably because
541 the DEM used to drape (overlay) the image on the terrain information was of low resolution.

542 ~~Third, the~~ The ultra-resolution (3×3 cm) image captured by ~~the the photographic camera flown on-~~
543 ~~board the~~ Unmanned Aerial Vehicle (UAV) proved to be very effective to detect and map the
544 landslide. The expert visual interpretation of the monoscopic ultra-resolution image provided
545 mapping results comparable to those obtained using the about 2-m resolution, ~~stereoscopic satellite~~
546 image.

547 ~~Fourth, a~~ comparative analysis of the technological constrains and the costs of acquisition and
548 processing of ultra-resolution imagery taken by UAV, and of high, or very-high resolution imagery
549 taken by optical satellites, revealed that the ultra-resolution images are well suited to map single
550 event landslides, clusters of landslides in a single slope, or a few landslides in nearby slopes in a
551 small area (up to few square kilometres, Giordan et al., 2017), and proved ~~unsuited~~ unsuited to cover large
552 and very large areas where the stereoscopic satellite images provide the most effective option
553 (Boccardo et al., 2015).

554 ~~Fifth, our~~ The field-based reconnaissance mapping (Map B) provided the least accurate mapping
555 results, measured by the largest mapping error (~~$E = 0.55$ for the entire landslide~~) when compared
556 to the benchmark map (~~Fig. 6~~). ~~Our~~ Results confirm the inherent difficulty in preparing accurate
557 landslide maps in the field through a reconnaissance mapping (Santangelo et al., 2010).

558 Although ~~we conducted our~~ the study was conducted on a single landslide (Fig. 1), ~~we maintain~~
559 ~~that~~ the findings are general, and can be useful to decide on the optimal imagery and technique to
560 be used when planning the production of a landslide inventory map. ~~We emphasize that the~~ The
561 technique and imagery used to prepare landslide inventory maps should be selected depending on
562 multiple factors, including (i) the typical or predominant landslide signature (photographic or
563 morphological), (ii) the scale and size of the study area (a single slope, a small catchment, a large
564 region), and (iii) the scope of the mapping (event, seasonal, multi-temporal, Guzzetti et al., 2012).

565 8 Acknowledgements

566 FF and MS were supported by a grant of Italian Dipartimento della Protezione Civile. We thank
567 Andrea Bernini and Mario Truffa, Servizio Protezione Civile della Città Metropolitana di Torino,

568 for flying the UAV over the Assignano landslide. Federica Fiorucci and Michele Santangelo
 569 designed the experiment and wrote this paper; Michele Santangelo mapped the landslide on the
 570 images, Mauro Rossi performed GPS survey, Daniele Giordan produced the UAV images. Fausto
 571 Guzzetti supervised the work, Federica Fiorucci, Daniele Giordan, Mauro Rossi, and Furio Dutto
 572 participated to field activities.
 573 Disclaimer. In this work, use of copyright, brand, logo and trade names is for descriptive and
 574 identification purposes only, and does not imply an endorsement from the authors or their
 575 institutions.

576 9 References

- 577 Allasia, P., Manconi, A., Giordan, D., Baldo, M., and Lollino, G.: ADVICE: a new approach for near-real-
 578 time monitoring of surface displacements in landslide hazard scenarios. *Sensors*, 13, 7, 8285-8302,
 579 <https://doi.org/10.3390/s130708285>, 2013.
- 580 Antonini, G., Ardizzone, F., Cardinali, M., Galli, M., Guzzetti, F. and Reichenbach, P.: Surface deposits
 581 and landslide inventory map of the area affected by the 1997 Umbria-Marche earthquakes, *Boll. Soc.*
 582 *Geol. It.*, 121, 843-853, 2002.
- 583 Ardizzone, F., Cardinali, M., Carrara, A., Guzzetti, F., and Reichenbach, P.: Impact of mapping errors on
 584 the reliability of landslide hazard maps, *Nat. Hazards Earth Syst. Sci.*, 2, 3-14,
 585 <https://doi.org/10.5194/nhess-2-3-2002>, 2002.
- 586 Ardizzone, F., Cardinali, M., Galli, M., Guzzetti, F., and Reichenbach, P.: Identification and mapping of
 587 recent rainfall-induced landslides using elevation data collected by airborne Lidar, *Nat. Hazards Earth*
 588 *Syst. Sci.*, 7, 637-650, <https://doi.org/10.5194/nhess-7-637-2007>, 2007.
- 589 Ardizzone, F., Fiorucci, F., Santangelo, M., Cardinali, M., Mondini, A.C., Rossi, M., Reichenbach, P., and
 590 Guzzetti, F.: Very-high resolution stereoscopic satellite images for landslide mapping. C. Margottini,
 591 P. Canuti, K. Sassa (Eds.), *Landslide Science and Practice, Landslide Inventory and Susceptibility*
 592 *and Hazard Zoning*, 1, Springer, Heidelberg, Berlin, New York, 95–101, [https://doi.org/10.1007/978-](https://doi.org/10.1007/978-3-642-31325-7_12)
 593 [3-642-31325-7_12](https://doi.org/10.1007/978-3-642-31325-7_12), 2013.
- 594 Boccardo, P., Chiabrando, F., Dutto, F., Tonolo, F.G., Lingua, A.: UAV deployment exercise for mapping
 595 purposes: evaluation of emergency response applications. *Sensors*, 15, 15717-15737, 2015,
 596 <https://doi.org/10.3390/s150715717>.
- 597 Brardinoni, F., Slaymaker, O., and Hassan, M.A.: Landslides inventory in a rugged forested watershed: a
 598 comparison between air-photo and field survey data, *Geomorphology*, 54, 179-196,
 599 [https://doi.org/10.1016/S0169-555X\(02\)00355-0](https://doi.org/10.1016/S0169-555X(02)00355-0), 2003.
- 600 Carrara, A., Cardinali, M., and Guzzetti, F.: Uncertainty in assessing landslide hazard and risk, *ITC Journal*,
 601 2, 172-183, 1992.
- 602 Di Maio, C., and Vassallo, R.: Geotechnical characterization of a landslide in a Blue Clay slope, *Landslides*,
 603 8, 17-32, <https://doi.org/10.1007/s10346-010-0218-8>, 2011.
- 604 Fiorucci, F., Cardinali, M., Carlà, R., Rossi, M., Mondini, A. C., Santurri, L., Ardizzone, F., and Guzzetti,
 605 F.: Seasonal landslides mapping and estimation of landslide mobilization rates using aerial and
 606 satellite images, *Geomorphology*, 129, 59-70, <https://doi.org/10.1016/j.geomorph.2011.01.013>,
 607 2011.

Formattato: Inglese (Regno Unito)

Formattato: Tipo di carattere: Corsivo, Inglese (Regno Unito)

Formattato: Inglese (Regno Unito)

Formattato: Inglese (Regno Unito)

- 608 Fiorucci, F.; Ardizzone, F.; Rossi, M.; Torri, D.: The Use of Stereoscopic Satellite Images to Map Rills and
609 Ephemeral Gullies. *Remote Sens.*, 7, 14151-14178, <https://doi.org/10.3390/rs71014151>, 2015.
- 610 Galli, M., Ardizzone, F., Cardinali, M., Guzzetti, F., and Reichenbach, P.: Comparing landslide inventory
611 maps, *Geomorphology*, 94, 268–289, <https://doi.org/10.1016/j.geomorph.2006.09.023>, 2008.
- 612 Giordan, D., Allasia, P., Manconi, A., Baldo, M., Santangelo, M., Cardinali, M., Corazza, A., Albanese, V.,
613 Lollino, G., and Guzzetti, F.: Morphological and kinematic evolution of a large earthflow: The
614 Montaguto landslide, southern Italy, *Geomorphology*, 187, 61-79,
615 <https://doi.org/10.1016/j.geomorph.2012.12.035>, 2013.
- 616 Giordan, D., Manconi, A., Allasia, P., and Bertolo, D.: Brief Communication: On the rapid and efficient
617 monitoring results dissemination in landslide emergency scenarios: the Mont de La Saxe case study,
618 *Nat. Hazards Earth Syst. Sci.*, 15, 2009-2017, <https://doi.org/10.5194/nhess-15-2009-2015>, 2015a.
- 619 Giordan, D., Manconi, A., Facello, A., Baldo, M., dell'Anese, F., Allasia, P., and Dutto, F.: Brief
620 Communication: The use of an unmanned aerial vehicle in a rockfall emergency scenario, *Nat.*
621 *Hazards Earth Syst. Sci.*, 15, 163-169, <https://doi.org/10.5194/nhess-15-163-2015>, 2015b.
- 622 Giordan, D., Manconi, A., Remondino, F., Nex, F.: Use of unmanned aerial vehicles in monitoring
623 application and management of natural hazards, *Geomatics, natural hazards and risk*, 8(1), 1-4, 2017.
- 624 Gokceoglu, C., Sonmez, H., Nefeslioglu, H. A., Duman, T. Y., Can, T.: The 17 March 2005 Kuzulu
625 landslide (Sivas, Turkey) and landslide-susceptibility Map of its near vicinity. *Engineering Geology*,
626 81, 1, 65-83, <https://doi.org/10.1016/j.enggeo.2005.07.011>, 2005.
- 627 Guzzetti, F., Cardinali, M., Reichenbach, P., Cipolla, F., Sebastini, C., Galli, M., and Salvati, P.: Landslides
628 triggered by the 23 November 2000 rainfall event in the Imperia Province, Western Liguria, Italy,
629 *Eng. Geol.*, 73, 229–245, <https://doi.org/10.1016/j.enggeo.2004.01.006>, 2000.
- 630 Guzzetti, F., Mondini, A. C., Cardinali, M., Fiorucci, F., Santangelo, M., and Chang, K.-T.: Landslide
631 inventory maps: new tools for and old problem, *Earth-Sci. Rev.*, 112, 42-66,
632 <https://doi.org/10.1016/j.earscirev.2012.02.001>, 2012.
- 633 Haneberg, W. C., Cole, W. F., and Kasali, G.: High-resolution lidarbased landslide hazard mapping and
634 modeling, UCSF Parnassus Campus; San Francisco, USA, *B. Eng. Geol. Environ.*, 68, 263-276,
635 <https://doi.org/10.1007/s10064-009-0204-3>, 2009.
- 636 Hutchinson, J. N.: A coastal mudflow on the London clay cliffs at Beltinge, North Kent, *Geotechnique*, 24,
637 412–438, 1970.
- 638 Manconi, A., Casu, F., Ardizzone, F., Bonano, M., Cardinali, M., De Luca, C., Gueguen, E., Marchesini,
639 Parise, M., Vennari C., Lanari, R., Lanari, R.: Brief Communication: Rapid mapping of landslide
640 events: the 3 December 2013 Montescaglioso landslide, Italy. *Natural Hazards and Earth System*
641 *Sciences*, 14, 7, 1835, <https://doi.org/10.5194/nhess-14-1835-2014>, 2014.
- 642 Mondini, A. C., Marchesini, I., Rossi, M., Chang, K.-T., Pasquariello, G., and Guzzetti, F.: Bayesian
643 framework for mapping and classifying shallow landslides exploiting remote sensing and topographic
644 data, *Geomorphology*, 201, 135-147, <https://doi.org/10.1016/j.geomorph.2013.06.015>, 2013.
- 645 Monserrat, O. and Crosetto, M.: Deformation measurement using terrestrial laser scanning data and least
646 squares 3D surface matching. *ISPRS J. Photogramm.*, 63(1), 142–154,
647 <https://doi.org/10.1016/j.isprsjprs.2007.07.008>, 2008.
- 648 Niculiță, M.: Automatic landslide length and width estimation based on the geometric processing of the
649 bounding box and the geomorphometric analysis of DEMs, *Nat. Hazards Earth Syst. Sci.*, 16, 2021-
650 2030, <https://doi.org/10.5194/nhess-16-2021-2016>, 2016.
- 651 Niethammer, U., S. Rothmund, M. R. James, Travelletti, J. and Joswig M.: UAV based remote sensing of
652 landslides, *Int. Arch. Photogram. Remote Sensing Spatial Info. Sci.*, 38(5), 496-501, 2010.

- 653 Petschko, H.; Bell, R. Glade, T.: Effectiveness of visually analyzing LiDAR DTM derivatives for earth and
654 debris slide inventory mapping for statistical susceptibility modeling, *Landslides* 13(5), 857-872,
655 2016, <https://doi.org/10.1007/s10346-015-0622-1>.
- 656 Pike, R.J.: The geometric signature: quantifying landslide-terrain types from digital elevation models,
657 *Mathematical Geology*, 20, 5, 491-511, 1988.
- 658 Plank, S.: Rapid damage assessment by means of multi-temporal SAR—A comprehensive review and
659 outlook to Sentinel-1, *Remote Sensing*, 6, 6, 4870-4906, <https://doi.org/10.3390/rs6064870>, 2014.
- 660 Razak, K. A., Santangelo, M., Van Westen, C. J., Straatsma, M. W., and de Jong, S. M.: Generating an
661 optimal DTM from airborne laser scanning data for landslide mapping in a tropical forest
662 environment, *Geomorphology*, 190, 112-125, <https://doi.org/10.1016/j.geomorph.2013.02.021>, 2013.
- 663 Rosi, A., Vannocci, P., Tofani, V., Gigli, G., Casagli, N.: Landslide characterization using satellite
664 interferometry (PSI), geotechnical investigations and numerical modelling: the case study of Ricasoli
665 Village (Italy). *Int. J. Geosci.*, 4, 904-918, <https://doi.org/10.4236/ijg.2013.45085>, 2013.
- 666 Santangelo, M., Cardinali, M., Rossi, M., Mondini, A. C., and Guzzetti, F.: Remote landslide mapping using
667 a laser rangefinder binocular and GPS, *Nat. Hazards Earth Syst. Sci.*, 10, 2539-2546,
668 <https://doi.org/10.5194/nhess-10-2539-2010>, 2010.
- 669 Santangelo, M., Marchesini, I., Bucci, F., Cardinali, M., Fiorucci, F., and Guzzetti, F.: An approach to
670 reduce mapping errors in the production of landslide inventory maps, *Nat. Hazards Earth Syst. Sci.*,
671 15, 2111-2126, <https://doi.org/10.5194/nhess-15-2111-2015>, 2015a.
- 672 Santangelo, M., Marchesini, I., Cardinali, M., Fiorucci, F., Rossi, M., Bucci, F., Guzzetti, F. A method for
673 the assessment of the influence of bedding on landslide abundance and types. *Landslides* 12, 295–
674 309. doi:10.1007/s10346-014-0485-x, 2015b.
- 675 Tarchi, D., Casagli, N., Fanti, R., Leva, D. D., Luzi, G., Pasuto, A., Pieraccini, M., Silvano, S.: Landslide
676 monitoring by using ground-based SAR interferometry: an example of application to the Tessina
677 landslide in Italy. *Eng. Geol.*, 68, 1, 15-30, [https://doi.org/10.1016/S0013-7952\(02\)00196-5](https://doi.org/10.1016/S0013-7952(02)00196-5), 2003.
- 678 Teza, G., Galgaro, A., Zaltron, N., Genevois, R.: Terrestrial laser scanner to detect landslide displacement
679 fields: a new approach. *Int. J. Remote Sensing*, 28, 16, 3425-3446,
680 <https://doi.org/10.1080/01431160601024234>, 2007.
- 681 Torrero, L. Seoli, L. Molino, A. Giordan, D. Manconi, A. Allasia, P. and Baldo, M. The Use of Micro-UAV
682 to Monitor Active Landslide Scenarios, in: *Engineering Geology for Society and Territory*, edited by:
683 Lollino, G., Manconi, A., Guzzetti, F., Culshaw, M., Bobrowsky P., and Luino, F., Springer
684 International Publishing Switzerland, 5, 701-704, https://doi.org/10.1007/978-3-319-09048-1_136,
685 2015.
- 686 Turner, D.; Lucieer, A. de Jong, S. M.: Time Series Analysis of Landslide Dynamics Using an Unmanned
687 Aerial Vehicle (UAV), *Remote Sensing* 7(2), 1736-1757, 2015, <https://doi.org/10.3390/rs70201736>.
- 688 Van Den Eeckhaut, M., Poesen, J., Verstraeten, G., Vanacker, V., Nyssen, J., Moeyersons, J., van Beek, L.
689 P. H., and Vandekerckhove, L.: Use of LIDAR-derived images for mapping old landslides under
690 forest, *Earth Surf. Proc. Land.*, 32, 754-769, <https://doi.org/10.1002/esp.1417>, 2007.
- 691
- 692

693
 694 **Table 1.** Characteristics of the images used to identify and map the Assignano landslide (Fig. 2).
 695 O: order in the sequence of images shown to the interpreter. Platform used to capture the image:
 696 W, WorldView-2 satellite; U, UAV. Resolution (ground resolution), ~~in metre~~. Spectral (image
 697 spectral composite): TCC, True Colour Composite (Red, Green, Blue); FCC, False Colour
 698 Composite (Near infrared, Red, Green). Type (image type): M, monoscopic; S, stereoscopic; P,
 699 pseudo-stereoscopic. Map: Corresponding landslide map (Fig. 5).

700

O	Platform	Resolution (m)	Spectral	Type	Map
1	W	1.84	TC	M	C
2	W	1.84	FCC	M	D
3	W	1.84	TC	S	E
4	W	1.84	FCC	S	F
5	U	0.03	TC	M	G
6	U	0.03	TC	P	H

701

702

Tabella formattata

703 **Table 2.** Comparison of the total landslide area (A_L), the landslide source and transportation area
 704 (A_{LS}), the landslide deposit (A_{LD}), the width and length of the entire landslide (W_L , L_L), of the
 705 source and transportation area (W_{LS} , L_{LS}), and of the deposit (W_{LD} , L_{LD}), for eight separate and
 706 independent cartographic representations of the Assignano landslide. EL, entire landslide; ST,
 707 landslide source and transport area; LD, landslide deposit. See **Table 3** for the characteristics of the
 708 single maps.

709

		Map A	Map B	Map C	Map D	Map E	Map F	Map G	Map H
Landslide area (m^2)									
EL	A_L	1.11×10^4	1.91×10^4	1.53×10^4	1.52×10^4	1.09×10^4	1.06×10^4	1.19×10^4	1.16×10^4
ST	A_{LS}	5.40×10^3	7.40×10^3	3.64×10^3	4.02×10^3	5.71×10^3	6.03×10^3	5.21×10^3	5.70×10^3
LD	A_{LD}	5.73×10^3	1.17×10^4	1.16×10^4	1.12×10^4	5.15×10^3	4.59×10^3	6.70×10^3	5.87×10^3
Landslide length (L_L , m) and width (W_L , m)									
EL	W_L	70.7	97.8	113.4	109.9	61.4	61.25	89.9	85.3
	L_L	362.0	387.5	404.7	391.2	354.6	359.5	343.3	349.1
ST	W_{LS}	51.5	59.6	43.6	49.2	51.92	54.3	49.5	50.5
	L_{LS}	227.9	229.7	205.9	208.0	239.0	239.2	234.7	237.3
LD	W_{LD}	61.0	98.69	111.5	109.0	56.0	57.6	89.9	81.9
	L_{LD}	152.7	172.1	206.2	203.5	129.8	134.7	139	121.8

710

711

Tabella formattata

Tabella formattata

Formattato: Inglese (Regno Unito)

Formattato: Inglese (Regno Unito)

712 **Table 3.** Comparison of the estimated cost, acquisition and pre-processing time, and storage
 713 requirement for an area of 4 km² (2 km × 2 km) and for an area of 100 km² (10 km × 10 km), for
 714 monoscopic and stereoscopic satellite images, and for an area of 15 km² for photographic images
 715 captured by an UAV.

716

	Satellite monoscopic		Satellite stereoscopic		UAV	
	4 km ²	100 km ²	4 km ²	100 km ²	4 km ²	15 km ²
Acquisition cost (€)	1.500	1.500	3.500	3.500	1.000	3.000
Pre-processing cost (€)	50	50	50	50	250-300	3.000
Acquisition time (day/person)	7-60	7-60	7-60	7-60	1	4
Pre-processing time (hr/person)	1	1	1	1	5-6	20-24
Storage (GB)	0.5	0.5	1	1	12	50
Resolution (m)	2	2	2	2	0.02	0.02
Morphologic signature	no	no	yes	yes	yes	yes
Photographic signature	yes	yes	yes	yes	yes	yes

717

718

719

720 **Figure captions**

721 **Figure 1.** The Assignano landslide, located near Collazzone, Umbria, central Italy. (A) global view
722 of the landslide. (B) detail of the landslide source area. (C) detail of the landslide transportation
723 area. (D) detail of the landslide deposit. Base image obtained overlaying (“draping”) the image on
724 Google Earth™. Red line is the boundary of the landslide obtained using the RTK ~~DGPS~~dGPS
725 (benchmark).

726 **Figure 2.** Images used to map the Assignano landslide. (A) TC WordView-2 satellite image, (A-
727 I) detail of the source area and (A-II) detail of the landslide deposit. (B) WordView-2 satellite
728 image in FCC, (B-I) detail of the source area and (B-II) detail of the landslide deposit. (C) UAV
729 monoscopic image and C-I a detail of the source area and C-II a detail of the deposition area.

730 **Figure 3.** Position of the seven GCPs used to evaluate the co-registration of WordView-2 satellite
731 image (A) and UAV image (B). Corresponding points are illustrated with the same symbol.
732 Differences of the coordinates of the corresponding points along X (~~i.e.~~, E-W direction, ΔX) and
733 along Y (~~i.e.~~, N-S direction, ΔY) are provided in metres on the left of the figure.

734 **Figure 4.** (A) Overview of the Assignano landslide area in Google Earth™ taken on 8 July 2013.
735 Photo shooting points and photograph taken (B) close to the landslide and (C) from a viewpoint.
736 The photographs taken in the field and the Google Earth™ image were used to prepare the
737 reconnaissance field map.

738 **Figure 5.** Eight independent cartographic representations of the Assignano landslide, “Map A” to
739 “Map H”. Map A obtained through a RTK ~~DGPS~~dGPS survey is considered the “benchmark”, and
740 shown as a thick black line in the other maps. Map B obtained through reconnaissance field
741 mapping. Map C to Map F obtained through the expert visual interpretation of the satellite images.
742 Map G and Map H obtained through the expert visual interpretation of the orthorectified image
743 taken by the UAV. See **Table 1** for image characteristics. Dark colours show the landslide source
744 and transportation area. Visual inspection of the images reveals the maps most similar to the
745 benchmark.

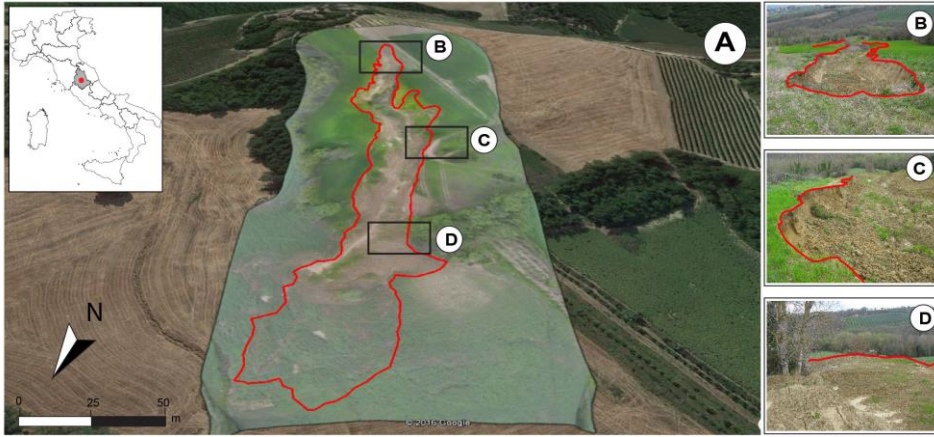
746 **Figure 6.** The error index (E) proposed by Carrara et al. (1992), was used to compare quantitatively
747 the different landslide maps. (I) Error index matrix for the landslide source and transportation area.
748 (II) Error index matrix for the landslide deposit. (III) Error matrix for the entire landslide. E spans

749 the range from 0 (perfect matching) to 1 (complete mismatch).

750 **Figure 7.** Comparison of landslide maps prepared for the Assignano landslide, Umbria, Central
751 Italy. (A) Landslide map obtained from a monoscopic (Map C, dark yellow line) and a stereoscopic
752 (Map E, light blue line), true-colour (TC) WordView-2 satellite image (base image), and a mapping
753 of the landslide obtained by walking a GPS receiver along the landslide boundary (Map A, black
754 line). (B) Landslide map obtained from a monoscopic (Map D, yellow line) and a stereoscopic
755 (Map F, cyan line), false-colour-composite (FCC) WordView-2 satellite image, and a mapping
756 obtained by walking a GPS receiver along the landslide boundary (Map A, black line). (C)
757 Landslide map obtained from field survey (Map B, pink line) and from a monoscopic, TC, ultra-
758 resolution image captured by an UAV (Map G, purple line), and the mapping obtained by walking
759 a GPS receiver along the landslide boundary (Map A, black line).

760

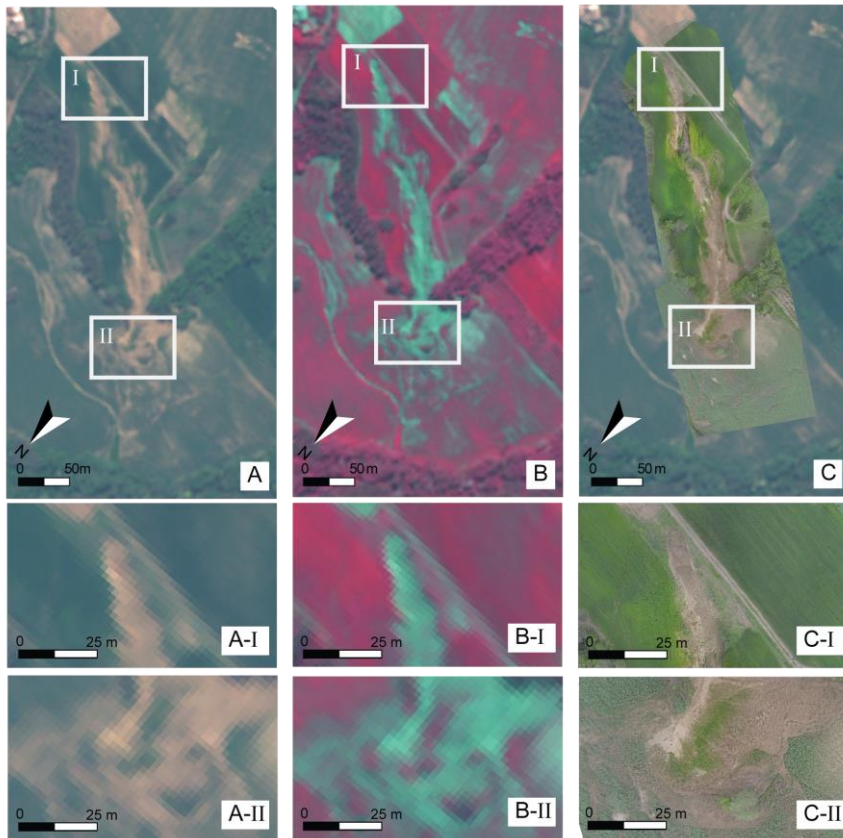
761 **Figure 1**



762

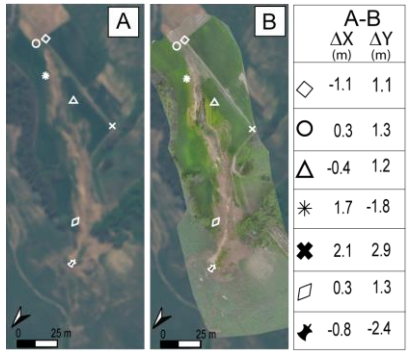
763

764 **Figure 2**



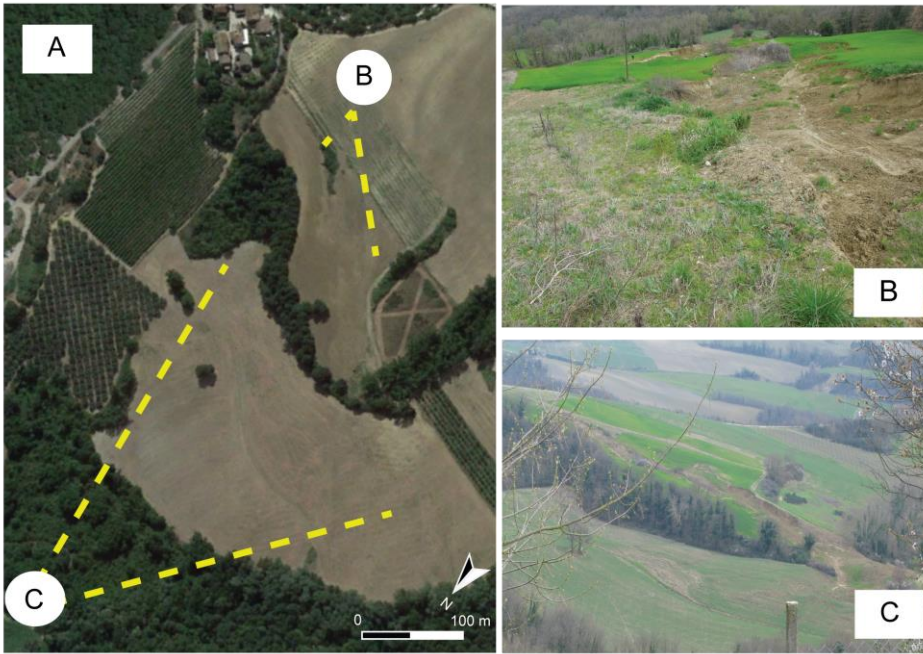
765

766 **Figure 3**
767



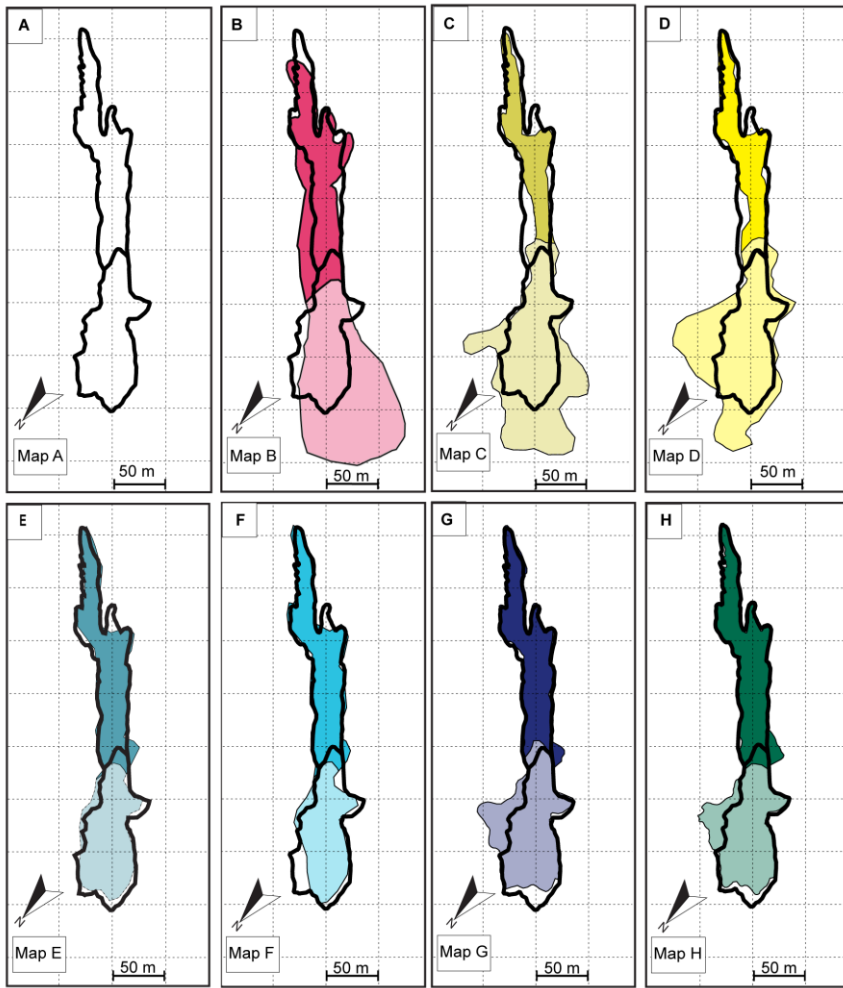
768

769 **Figure 4**



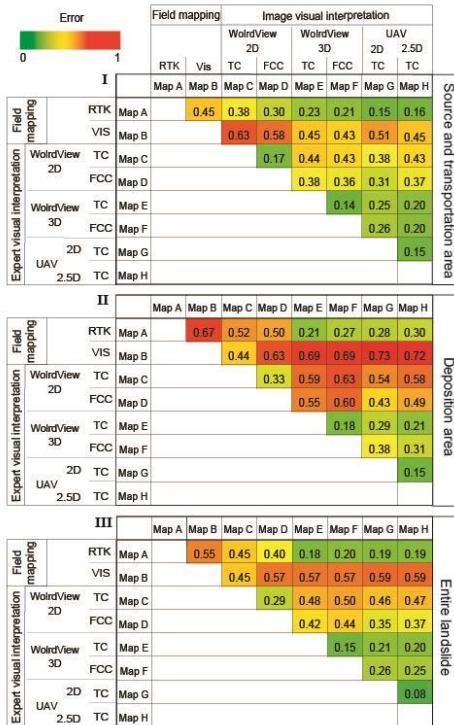
770

771 **Figure 5**



772

773 **Figure 6**

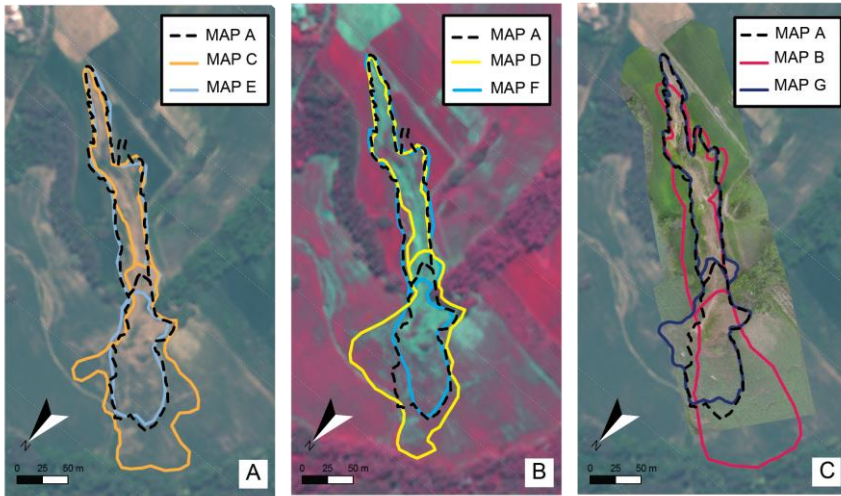


774

775

776

777 **Figure 7**



778